Excerpt from the Proceedings of the 2011 COMSOL Conference in Boston

The Role of 1D & 2D Asymmetric Diffusion Layers in Rectification Through Ion-Selective Membranes

Will Booth[1*], Jarrod, Schiffbauer[1], and Boyd Edwards[2]
[1]*Physics Department, West Virginia University*
[2]*Physics Department, Utah State University and*
**Corresponding author: 3288 University Avenue, APT 402, Morgantown, WV 26505. wbooth@mix.wvu.edu*

Abstract

Our computational model consists of an ion-selective membrane in series with micro-channels filled with a binary aqueous electrolyte solution. When an electric field is applied across this system ion diffusion layers (DLs) form on each side of the membrane in the channels. The electric current through the system is strongly dependent on the geometry of these DLs. We investigate theoretically how 1D and 2D diffusion layer geometries compare in their effects on ionic current rectification through non-ideal ion-selective membranes. It is found that radial flux focusing into the membrane from a larger 2D channel acts similarly to a shortened 1D diffusion layer. The role of the inner membrane diffusion on the current-voltage curves is also illuminated. Finally, we briefly investigate the roles membrane charge, the membrane diffusivity, and the EDL length play.

I. INTRODUCTION

Ion-selective membranes often come in the form of a charged nano-porous membrane and are typically placed in series with two micro-fluidic channels. Within the pores electric double layers (EDLs) overlap and inhibit the presence of co-ions (ions with the same charge as the membrane). These systems display unique current characteristics depending on ion concentration, voltage, membrane charge, and geometry [1–5]. They are investigated for applications in desalination [6] and as components of biosensors[7]. However, much of the transport behavior is still requires understanding. Fluid vortices of various types often pose problems as they can be difficult to distinguish from one another. These can include pressure driven vortices due to sudden change in channel cross section, vortices from induced-charge electroosmosis (ICEO) occurring around conducting surfaces [8], and non-equilibrium electroosmotic instabilities occurring from small perturbations [9]. Finally, one can also generate vortices due to the non-linear electroosmotic slip velocity on charge-selective surfaces [10]. Here we will be ignoring the fluid flow however and focus on how geometric asymmetries affect the electro-diffusion of the ions.

Figure 1 shows examples of the 1D and 2D systems

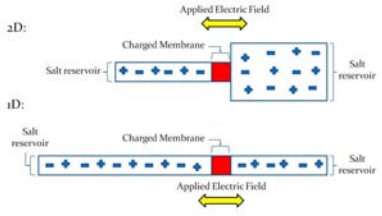

Figure 1: 1D and 2D model geometries. Make better figure that notes boundary conditions. Remove + and - symbols. Remember half of the applied potential is at each side of system. Also add a small set of x, y axes.

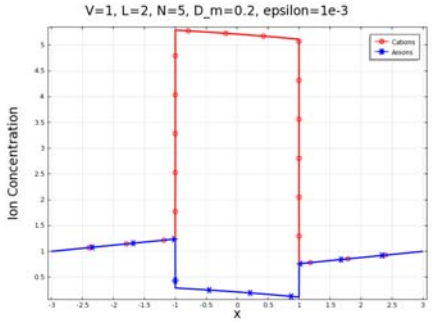

Figure 2: 1D Concentration profile with symmetric diffusion layers in a steady state for a 1:1 electrolyte solution. The membrane is treated as a region of fixed negative charge density N $(= 5)$. Cations are red with circles and anions are blue with asterisks. Fluid flow is neglected and so the system is purely electro-diffusive. The membrane extends from $x = (-1, 1)$. The inset shows the EDL close up. Include plot of potential profiles later.

used in our computer modeling along with the boundary conditions. (The specifics of the models are discussed in section II. In equilibrium the ion concentrations are at the bulk reservoir value everywhere except in the membrane where the counter-ions are enhanced and co-ions are depleted. At the interface of the membrane and micro-channel there are small EDLs. If a weak electric field is applied, for example, to the left then anions will build up on the left side of the negatively charged membrane. See Fig. 2 for the case of a 1D system with symmetric DLs. As the solution attempts to remain electroneutral the cations will also be enriched here. Meanwhile both ion concentrations will be depleted on the right side as the anions fail to be resupplied through the membrane. Steady-state is obtained as the co-ion (anion) diffusive flux balances out the oppositely directed co-ion electro-migration.

As the applied voltage is increased the concentration gradients in the DLs increase as well, thus lowering the

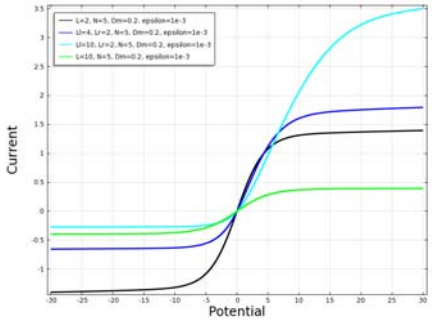

Figure 3: 1D I-V curves.

concentration on the right side of the membrane and increasing it on the left in the case of Fig. 2. This is also called concentration polarization (CP) [11]. The current will likewise increase as the concentration goes toward zero in the depleted region. As the concentration cannot drop below zero in the depleting region the current will plateau at a threshold voltage before local electroneutrality begins to break down in this DL and a space-charge layer (SCL) forms allowing the current to slowly continue increasing with applied voltage [2, 12, 13]. See the black curve Fig. 3 for the I-V curve for this case.

Much of the behavior is tied to the length of the diffusion layers which form in the microchannels flanking the membrane [2, 3, 5]. The co-ion diffusive flux acts against their electro-migration and so the co-ions contribute little to the current. The diffusive flux of the counter-ions in the DLs acts with their electro-migration though. So smaller DLs imply larger concentration gradients, greater diffusive flux of counter-ions, and thus greater current. Adding higher dimensions instead of simply changing the extent of the DL in the computational model will of course change the geometry of the DL in a different way. Allowing asymmetry in the 1D and 2D DLs will induce a current rectification effect with an "on-state" and "off-state" as if the system were a diode.

II. COMPUTATIONAL MODELS

The system is modeled with Poisson's equation for electrostatics (Electrostatics Module) and the Nernst-Planck equations (Transport of Diluted Species Module) for the conservation of each ion species. The equations are nondimensionalized for generality and simplicity. Variables with a tilde overhead are unscaled. Poisson's equations reads as

$$-\varepsilon^2\nabla^2\phi = p - n - N\left(\vec{x}\right) \tag{1}$$

where $\phi = e\widetilde{\phi}/k_BT$ is the scaled electric potential, $p = \widetilde{p}/c_0$ is the scaled cation concentration, $n = \widetilde{n}/c_0$ is the scaled anion concentration, $N\left(\vec{x}\right) = \widetilde{N}\left(\vec{x}\right)/c_0$ is the scaled fixed negative charge density in the membrane, $\nabla^2 = \delta^2\widetilde{\nabla}^2$ is the scaled Laplacian operator, and $\varepsilon = \sqrt{dk_BT/c_0e^2\delta^2}$ is the scaled Debye length or EDL length. Here e is the electron charge, k_BT is the thermal energy, c_0 is the bulk ion concentration, d is the dielectric permittivity of the system, and δ is the membrane half-length. The membrane charge density $N\left(\vec{x}\right)$ is 0 everywhere except inside the membrane where it is called simply N.

The continuity equations read as

$$\vec{\nabla}\cdot D\left(\vec{x}\right)\left[-\vec{\nabla}c_i - z_ic_i\vec{\nabla}\phi\right] = \vec{\nabla}\cdot\vec{j}_i = \frac{\partial c_i}{\partial t}, \quad i = p,\, n \tag{2}$$

where $c_{p,\,n} = p,\, n$ is the scaled concentration for each ion species, $\vec{j}_i = \frac{\delta\tilde{j}_i}{\widetilde{D}c_0}$ is the scaled species flux, $z_{p,\,n} = +1, -1$ is the species charge number, and $t = \frac{\tilde{t}\tilde{D}}{\delta^2}$ is the time nondimensionalized by a membrane diffusion time-scale. $\tilde{D}$ is the diffusivity of each ion species and $D\left(\vec{x}\right)$ is the scaled diffusivity defined piecewise as 1 everywhere except in the membrane where it is 0.2 to account for tortuousity of the membrane. In the steady-state this becomes

$$\vec{\nabla}\cdot D\left(\vec{x}\right)\left[-\vec{\nabla}c_i - z_ic_i\vec{\nabla}\phi\right] = 0 \tag{3}$$

as $\frac{\partial c_i}{\partial t} = 0$.

Boundary conditions are as in Fig. 1. The concentrations for each species are set at $c_i = 1$ at each end of the two microchannels. This represents either the salt reservoir which holds the terminals or the end of a fluid vortex stirring in the salt. A potential bias of $-V/2$ is applied on the left end and $V/2$ on the right end. In 2D all other boundaries (aside from the continuous interior boundaries) have no potential gradient and no normal flux allowed as

$$\hat{n}\cdot\vec{\nabla}\phi = 0, \quad \hat{n}\cdot\vec{j}_i = 0. \tag{4}$$

where $\hat{n}$ is the unit vector normal to the surface.

In 1D the current density is evaluated as $i = j_p - j_n$. In 2D the current is evaluated by integrating the current density i over the end microchannel boundary which remains constant in each 2D model to attain the current I.

We used COMSOL 4.2 for the steady-state finite element calculations performed here. In the 1D model a high-quality mesh is specified near the membrane-microchannel boundaries to resolve the small EDLs. In 2D a mapped quadrilateral element mesh is created at the membrane-microchannel interfacial boundary again to resolve the EDLs. In 1D away from these boundaries a lower element density is specified in the membrane in microchannels which scales with the size of the model. In 2D outside the EDL boundaries a free triangular element meshing program within COMSOL is used. Different meshing qualities were tested in order to ensure accuracy of the models presented. The 2D model consisted of only the top half of the 2D diagram shown in Fig. 1 and symmetry was assumed across the new bottom boundary (i.e. the center-line of the channels and membrane.) This consisted of using the same boundary conditions here as in Eqn. 4.

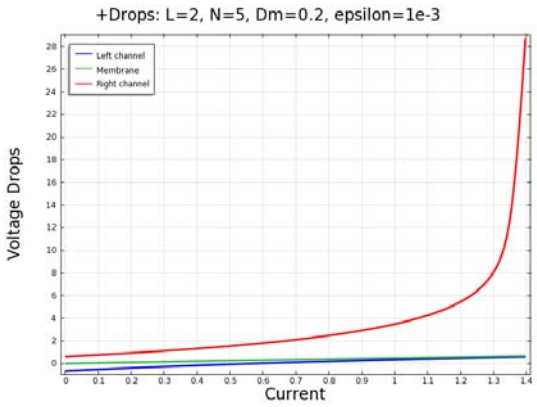

Figure 4: Potential drops across components of the $L = 2$ symmetric system plotted against current.

III. RESULTS AND DISCUSSION

In [17] 1D calculations for a very similar system were performed using a small EDL approximation. As such local electroneutrality (LEN) is assumed throughout the system and matching boundary conditions are used across the membrane-microchannel interface. As noted in Section II we now make no such approximations for LEN. Unless otherwise noted the value of the half-membrane thickness is set as $\delta = 1$, the fixed membrane negative charge density is set as $N = 5$ and the EDL length scale is $\varepsilon = 10^{-3}$. The length of the left and right microchannels, effectively the DL lengths, will be designated by L_l and L_r respectively. In 2D the height of the left and right microchannel will be designated by H_l and H_r respectively. The height of the membrane H_m in 2D will be equal to H_l and each of these heights will remain constant at $H_{l,m} = 0.1$ throughout the 2D models as H_r varies. The lengths of the 2D channels will also be constants as $L_{l,r} = 4$.

A. 1D Rectification

As can be seen from Fig. 3 comparing the black and green 1D I-V curves where the DLs are symmetric with $L_{l,r} = L = 2$ and $L_{l,r} = L = 10$ respectively the case of shorter DL lengths always has a higher current. This is for the reasons described in Section I. The shorter DLs provide a larger cation diffusive current. Additionally a smaller DL essentially implies a lower total resistance for the applied voltage and therefore a higher current. Most of the resistance comes from the depletion layer as a lower ion concentration implies a lower conductivity. This is demonstrated in Figs. 4 and 5 where positive potential is applied on the right and the depletion layer forms on the right side.

Fig. 6 shows the concentration profiles for the case of V above the threshold voltage value V_T (~ 8 for this set of parameters). V_T stands for the voltage region where

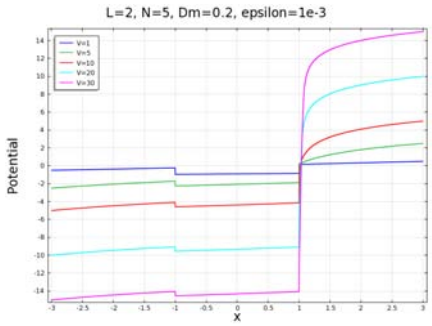

Figure 5: 1D symmetric system potential profiles. Note most of the potential drop occurs across the depletion layer from $x = 1$ to $x = 3$.

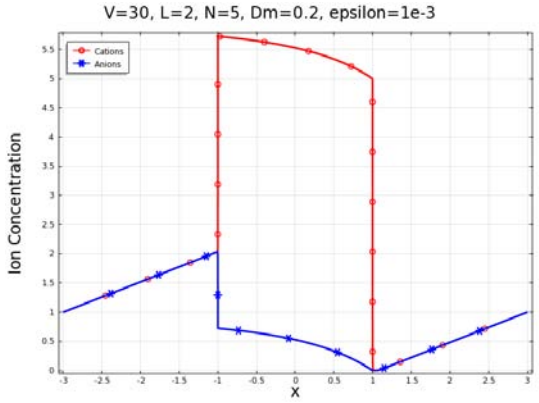

Figure 6: Concentration profiles for voltage above the critical value in a symmetric system. Cations are red with circles and anions are blue with asterisks. The inset shows the extended SCL as compared with the inset in Fig. 2.

the current begins to plateau. As V increases and the ion concentration in the depletion layer goes towards zero near the membrane. This would eventually prevent the current from increasing at all as is the case in LEN models and reach Levich's classical limiting current [14]. However here we have LEN break-down and an SCL forms as counter-ion (cation) concentration rises above the co-ion (anion) concentration allowing slow continuation of current increase with increasing V.

When the DLs are of differing lengths ($L_l \neq L_r$) the system will become a current rectifier as seen in 3 for the asymmetric DL cases; blue ($L_l = 4$ and $L_r = 2$) and cyan ($L_l = 10$ and $L_r = 2$). The on-state ($V > 0$) current for these asymmetric cases is also higher than the black symmetric case with ($L = 2$) shorter DLs. The off-state ($V < 0$) of the cyan case also has a current even lower than the green symmetric $L = 10$ case.

In the on-state (see Fig. 8) of our asymmetric systems ($L_l > L_r$ and $V > 0$) the ion concentrations and concentration gradients within the membrane can be very large. This is caused by the asymmetric diffusion of the counter-ions; large in the right channel and small in the left channel. Continuity will insist a counter-ion concen-

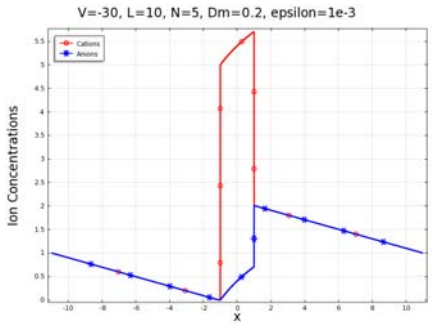

Figure 7: Symmetric system concentration profile above V_T.

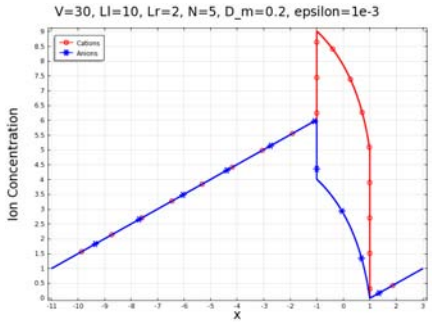

Figure 8: Concentration profiles for an asymmetric system with $V = 30,\ L_l = 10,\ L_r = 2$ above V_T in the on-state ($V > 0$).

tration gradient form in the membrane to balance this out. As the system attempts to remain electro-neutral though the co-ions will also attain a membrane concentration gradient. This yields a very large concentration for both ion species in the membrane when compared to the other cases. Large concentrations imply a greater conductivity to the system. Additionally the selectivity of the system, defined as the ratio of the counter-ion flux to the co-ion flux (j_p/j_n), will decrease as the co-ions begin to contribute more to the current due to their increase in membrane concentration and membrane diffusive flux. See Fig. 9. The magnitude of this increase in current due to these effects can easily be enough to cause the

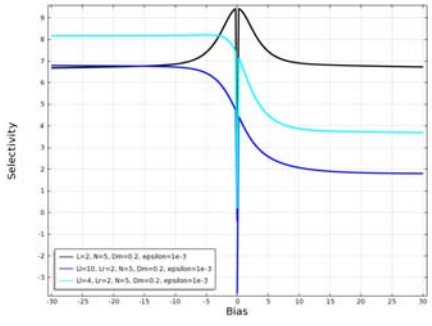

Figure 9: Selectivity (j_p/j_n) as a function of applied bias in 1D models.

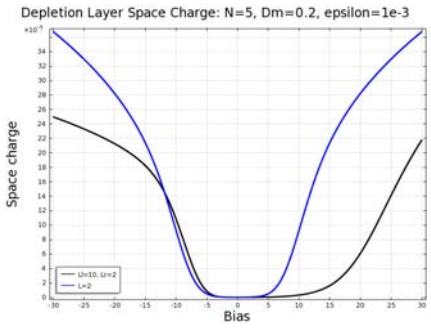

Figure 10: Space charge ($p - n$) in the depletion layer. In the on-state black asymmetric case we see the least amount of charge charge development, followed by the off-state, followed by the amount in the blue symmetric case over most voltages.

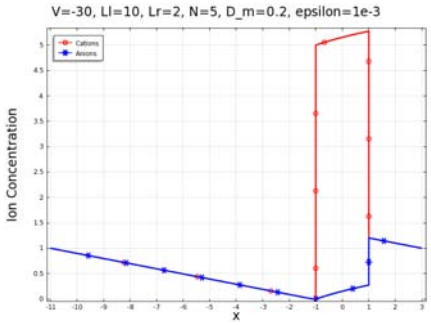

Figure 11: Concentration profiles for an asymmetric system with $V = -30,\ L_l = 10,\ L_r = 2$ above V_T in the off-state ($V < 0$).

on-state rectifier current to be larger than the symmetric cases (for large V). Compare the black, blue, and cyan cases of Fig. 3.

The depletion layer will fail to be depleted as quickly as a function of applied voltage because of the asymmetric DLs and the membrane diffusion. This can be seen by evaluating the total space charge throughout the channel with the depletion layer as seen in Fig. 10. As such V_T will be increased and the I-V curve will remain pseudo-Ohmic over a larger range of V, thus allowing the current to go higher. It is possible that this shift in V_T could also shift the point of formation of the various vortices [17].

The off-state of the asymmetric rectifier (see Fig. 11) will have a very low current for reasons opposite to that of the on-state having a high current. Here the counter-ions will build up even less of a gradient in the membrane than they would in the symmetric case. As such there will be lower current because of a decrease in conductivity and a decrease in selectivity as the co-ion flux contribution is weakened. See Fig. 9 again here. This is true even when comparing the cyan, $L_l = 10,\ L_r = 2$ and $V < 0$ system to the green $L_{l,r} = 10,\ V < 0$ system. This is why the off-state cyan case has an even lower current than the off-state green case.

For more on the 1D rectification theory see also [17].

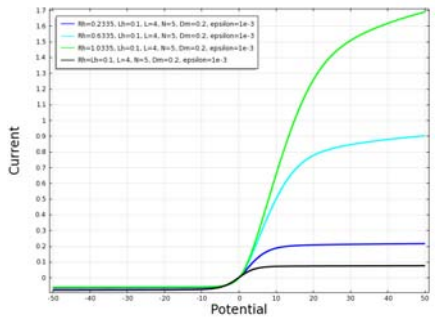

Figure 12: 2D I-V curves for varying H_r.

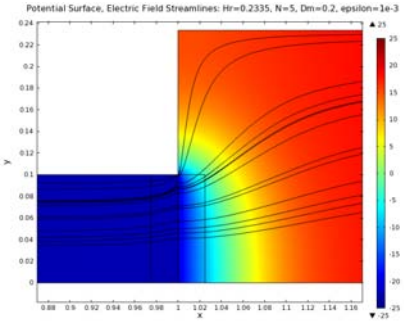

Figure 13: 2D Potential surface plot with electric field streamlines.

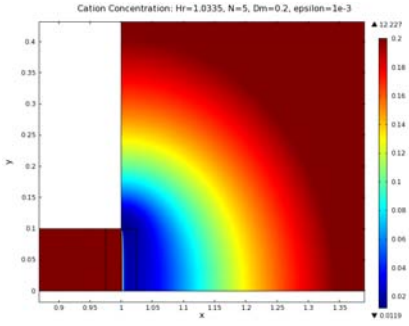

Figure 14: 2D Surface plot of the cation concentration. Dark red represents concentrations higher than 0.2. This is done to emphasize the radial focusing near the membrane.

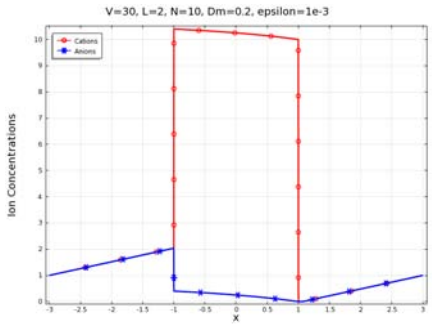

Figure 15: 1D concentration profiles for $N = 10$.

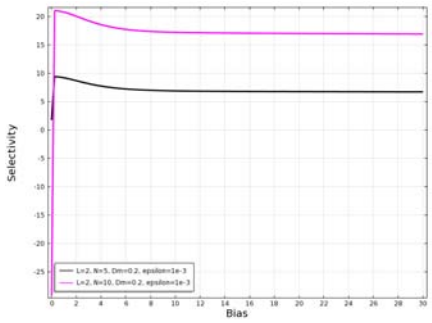

Figure 16: A plot of selectivity for two symmetric systems with $N = 5, 10$.

B. 2D Rectification

In the previous subsection we saw that changing the length of the DLs changes the I-V response of the system. However in real systems it is rare that the geometry is 1D. Often the system involves a nano-capillary membrane in series with microchannels. Thus we have radial field- and flux-focusing into small pores. The distance between these pores can vary from membrane to membrane as well, thus making cross-talk amongst them a possible issue. As discussed in [2, 3] the effect of the focusing into nano-pores can act as a way to shorten the effective DL length.

Fig. 12 shows the I-V curves for the 2D systems we modeled where H_l, and $L_{l,r} = L = 4$ are kept constant as H_r varies. We see that rectification indeed occurs in the expected direction. The right side microchannel height is increased and thus acts as a shorter DL due to the radial focusing. This is analogous to the 1D case where the left DL was set to be larger. Fig. 13 shows a surface plot of the potential along with the electric field streamlines near the membrane. Fig. 14 depicts the cation concentration near the membrane for a larger . This demonstrates the radial focusing occurring at the right pore mouth that acts to effectively shorten the DL here.

Many effects seen in the 1D models are seen here as well. V_T is shifted with increasing cross-section asymmetry. This suggests radial focusing can be used for the same purposes for controlling electrokinetic flow and possibly electroconvection as the 1D asymmetric DLs could.

C. Membrane Charge, Diffusivity, And EDL Length

The parameters N, D_m, and ε have been held constant throughout the models presented so far. Here we briefly present their effects on the system.

The membrane charge density N primarily controls the selectivity of the system. The higher N is the less co-ions (n, here) can flux through the system. Fig. 15 shows an example concentration profile and Fig. 16 shows the

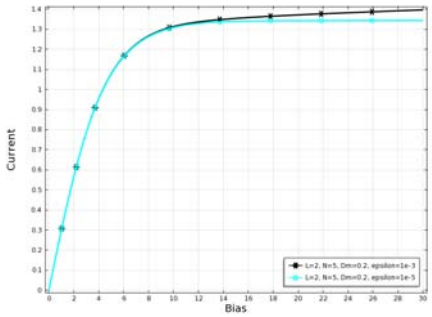

Figure 17: 1D I-V curves for varying EDL length scale, ε.

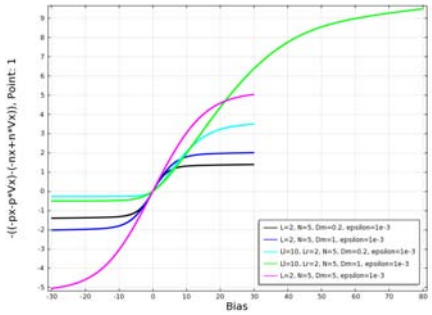

Figure 18: I-V curves for varying D_M.

selectivity with only N varying. The I-V curves look much like Fig. 3 aside from a lower current for all V.

As the EDL length scale parameter ε decreases in size the system more closely approximates a fully electroneutral system. This essentially reduces the extent of the space charge region outside of the membrane. As in the symmetric full LEN models in [17] the I-V become flatter beyond V_T with decreasing ε. This can be seen in Fig. 17. Adding asymmetry to the system does not change this trend.

Increasing membrane diffusivity will act to prevent the depletion layer from being depleted as much. As such the current will be able to remain pseudo-Ohmic over a greater range of V allowing for a larger current. This effect is amplified in the asymmetric case. See Fig. 18.

IV. ACKNOWLEDGMENTS

We would like to acknowledge the NSF DDEP program, WVSGC-NASA, WVU Research Corporation, and WVEPSCoR HEPC.dsr.09013. We would also like to thank Lloyd Carroll and Paul Cassak for helpful discussions.

[1] Derek Stein, Maarten Kruithof, and Cees Dekker, Surface-Charge-Governed Ion Transport in Nanofluidic Channels, *Physical Review Letters*, **93**, 1-4 (2004).

[2] Gilad Yossifon, Peter Mushenheim, Yu-Chen Chang, and Hsueh-Chia Chang, Nonlinear current-voltage characteristics of nanochannels, *Physical Review E*, ***79***, 1-9 (2009).

[3] Gilad Yossifon, Peter Mushenheim, Yu-Chen Chang, and Hsueh-Chia Chang, Eliminating the limiting-current phenomenon by geometric field focusing into nanopores and nanoslots, *Physical Review E,* **81**, 1-13 (2010).

[4] Hirofumi Daiguji, Yukiko Oka, and Katsuhiro Shirono, Nanofluidic Diode and Bipolar Transistor, *Nano Letters*, **5**, 2274-80 (2005).

[5] Ye Ai, Mingkan Zhang, Sang W. Joo, Marcos a. Cheney, and Shizhi Qian, Effects of Electroosmotic Flow on Ionic Current Rectification in Conical Nanopores, *The Journal Of Physical Chemistry C*, **114**, 3883-3890 (2010).

[6] Hsueh-Chia Chang and Gilad Yossifon, Understanding electrokinetics at the nanoscale: A perspective, *Biomicrofluidics*, 3, 12001 (2009).

[7] Howorka, S.; Siwy, Z., Nanopore analytics: sensing of single molecules, *Chem. Soc. ReV.*, **39**, 2009, 2360–2384.

[8] M. Jain, a. Yeung, and K. Nandakumar, Efficient Micromixing Using Induced-Charge Electroosmosis, *Journal of Microelectromechanical Systems*, **18**, 376-384 (2009).

[9] S. Rubinstein, G. Manukyan, a. Staicu, I. Rubinstein, B. Zaltzman, R. Lammertink, F. Mugele, and M. Wessling, Direct Observation of a Nonequilibrium Electro-Osmotic Instability, *Physical Review Letters*, **101**, 1-4 (2008).

[10] Y. Ben and H.C. Chang, Nonlinear Smoluchowski slip velocity and micro-vortex generation, *Journal of Fluid Mechanics*, **461**, 229–238 (2002).

[11] Qiaosheng Pu, Jongsin Yun, Henryk Temkin, and Shaorong Liu, Ion-Enrichment and Ion-Depletion Effect of Nanochannel Structures, *Nano Letters*, **4**, 1099–1103 (2004).

[12] E. a. Demekhin, E. M. Shapar', and V. V. Lapchenko, Initiation of Electroconvection in Semipermeable Electric Membranes, *Doklady Physics*, **53**, 450-453 (2008).

[13] B. Zaltzman and I. Rubinstein, Electro-osmotic slip and electroconvective instability, *Journal of Fluid Mechanics*, **579**, 173–226 (2007).

[14] V. Levich, *Physicochemical Hydrodynamics* (Prentice-Hall, 1962).

[15] S.J. Kim, Y.C. Wang, J.H. Lee, Hongchul Jang, and Jongyoon Han, Concentration Polarization and Nonlinear Electrokinetic Flow near a Nanofluidic Channel, *Physical Review Letters*, **99**, 44501 (2007).

[16] Isaak Rubinstein and Boris Zaltzman, Electro-convective versus electroosmotic instability in concentration polarization, *Advances In Colloid and Interface Science*, **134-135**, 190-200 (2007).

[17] Jarrod Schiffbauer, Will Booth, Kathleen Kelly, Boyd Edwards, and Aaron Timperman. In Preparation. (2011).